Received: 14 August 2025 | Revised: 3 February 2026 | Accepted: 23 April 2026 | Published online: 3 June 2026

RESEARCH ARTICLE

Journal of Data Science and Intelligent Systems
2026, Vol. 00(00) 1–19
DOI: 10.47852/bonviewJDSIS62027208

BON VIEW PUBLISHING

# High-Resolution Evaluation of WRF Cumulus Parameterization Schemes for Rainfall Prediction in Thailand

**Usa Wannasingha Humphries[1,*], Muhammad Waqas[2], Boonlert Archevarahuprok[3], Porntip Dechpichai[1], Angkool Wangwongchai[1] and Boobphachard Chansawang[1]**

[1] *Department of Mathematics, King Mongkut's University of Technology Thonburi, Thailand*

[2] *The Joint Graduate School of Energy and Environment, King Mongkut's University of Technology Thonburi, Thailand*

[3] *Climate Center, Thai Meteorological Department, Thailand*

**Abstract:** This study evaluates the performance of cumulus parameterization schemes under a default SBU-YLin within the weather research and forecasting (WRF) model to enhance rainfall forecasting in Thailand's tropical climate. Using a high-resolution nested domain setup (8.1 × 8.1 km, 2.7 × 2.7 km, and 0.9 × 0.9 km), simulations are validated against 128 Thai Meteorological Department stations from September 21 to 23, 2024. The New Tiedtke (RAIN-16) scheme achieved the most balanced performance, with underestimation and overestimation rates of approximately 50% and mean underestimation and overestimation of −12.75 mm and 13.30 mm, respectively. However, the SBU-YLin scheme reduced biases, root mean square error (RMSE), and mean absolute error (MAE) but could not resolve heavy rainfall events, especially in Domains 2 and 3, which are considered high-resolution domains. In Domain 1, very heavy rainfall was overestimated with an RMSE of 98.50 mm; Domain 2 showed an overestimation of rainfall, and Domain 3 had a substantial overestimation of rainfall associated with localized convective activity. However, the SBU-YLin scheme reduced the biases, RMSE, and MAE, but at higher computational demands. Results showed that Domains 2 and 3 increased accuracy with finer spatial resolution, but it was challenging to simulate heavy rainfall events. The selected 3 days are an intense rainfall event that is characteristic of monsoonal convection in Thailand. This brief time span enables WRF schemes to be examined at a resolution in extreme conditions. The temporal coverage of future research is going to be extended to a seasonal-level assessment.

**Keywords:** weather research and forecasting, rainfall prediction, cumulus parameterization schemes, numerical weather prediction

## 1. Introduction

Weather and climate are key factors in public health, economic activities, ecosystem stability, and governance at the global scale [1]. Variability and long-term shifts affect societal resilience, policy development, and strategies for sustainable growth. Typically, weather forecasting deals with short-term atmospheric conditions and climate modeling with long-term changes in atmospheric variables [2, 3]. With the rising frequency of global warming and climate change [1], there is a demand for accurate and timely predictions of extreme weather events and significant climate changes.

Rainfall prediction under extreme climate conditions represents one of the most challenging and critical meteorological tasks [1, 4]. Rainfall modeling is subject to many factors, including dynamic and thermodynamic characteristics of the atmosphere and microphysical processes [5]. The weather research and forecasting (WRF) model has become one of the most popular platforms for NWP because of its modularity and availability of various physical parametrization options for cumulus and microphysics schemes that describe the formation of clouds and convective activity at the sub-grid scale. These parameterizations are critical in defining the performance of rainfall predictions [6].

Cumulus parameterization schemes are projected to model the vertical transport of heat, moisture, and momentum due to convection in the troposphere [7]. These schemes become necessary when the model's grid resolution is insufficient to resolve these processes independently [8]. They switch on columns where convective instability is present and calculate tendencies for temperature, humidity, and the convective part of surface rainfall. Rising thermals take moist air parcels to the upper troposphere, where moisture condensation causes rainfall. At the same time, downdrafts caused by the evaporative cooling of rain bring mid-tropospheric air to the boundary layer, thus enhancing the stability of the column [9]. These processes in most WRF cumulus parameterization schemes, such as Kain–Fritsch (KF) (RAIN-1) and Grell–Freitas (GF) (RAIN-3), are modeled using mass-flux frameworks [10].

***Corresponding author:** Usa Wannasingha Humphries, Department of Mathematics, King Mongkut's University of Technology Thonburi, Thailand. Email: usa.wan@kmutt.ac.th

On the other hand, simpler adjustment-type schemes such as Betts–Miller–Janjic (BMJ) adjust the atmospheric profile toward a specified post-convective state [11]. Earlier studies provide vital information on the performance of cumulus parameterization schemes in different climates [12–14]. For example, the study conducted in the Yangtze River Delta, China, showed that the KF and BMJ schemes described the overall behavior of the rainfall during extreme rainfall, but the BMJ scheme was more accurate regarding the intensity and spatial distribution of the rainfall [8]. In addition, the comparison of KF and Grell-3D schemes in the Weihe River Basin, China, revealed that both schemes are good at simulating the distribution of rainfall but differ in the ability to reproduce the zones of heavy rainfall, with Grell-3D providing higher spatial resolution of the maximum values of rainfall intensity.

Microphysics schemes, in contrast, control the processes of formation, development, and interaction of cloud hydrometeors, which determine rainfall [8, 15, 16]. It has been found that the choice of microphysics schemes can influence the rainfall rates, their spatial distribution, and the time when they occur [17]. For example, the Thompson and Morrison schemes, which include double-moment representations, have shown better results in simulating mixed-phase processes and graupel in convective systems [18]. However, these elaborate structures are computationally complex, and the improvement in forecast accuracy is not always proportional to the computational complexity [15, 19, 20]. Likewise, sensitivity analyses over the Himalayas found the Thompson scheme best suited for monsoon-induced heavy rainfall, while the KF cumulus scheme was suitable for low-resolution domains [5].

While significant advancements have been made in the parameterization of the convective scale, there are still substantial uncertainties in modeling heavy rainfall [6, 21]. These uncertainties arise from problems associated with observational data sets, errors in initial and boundary conditions, and the stochastic nature of convective processes [18]. For example, grid-to-point comparisons in validation studies are confounded by spatial rainfall variability during a short-duration convective occurrence [22].

Satellite-derived rainfall products can also be helpful in validation, as they offer continuous spatial coverage, especially when rainfall data are scarce [21]. However, inconsistencies between observed and simulated rainfall remain challenging.

Thailand has an orographic impact that affects rainfall distribution in specific regions, necessitating a fine-scale simulation study. However, the use of cumulus parameterization schemes in Thailand is limited by the "gray zone" of the model resolutions [6, 23]. When grid sizes are coarser than 10 km, parameterization is necessary to approximate sub-grid-scale convective processes [24]. On the other hand, at a resolution finer than 3 km, it is possible to use explicit convection schemes only [25]. Nevertheless, the 3–10 km range remains problematic regarding the optimal specification of parameterization schemes [6]. For this reason, using the grid resolution of 8.1 × 8.1 km adopted in this study, evaluating the need and effectiveness of cumulus parameterization schemes is a crucial research direction.

This research aims to evaluate cumulus parameterization schemes at a grid resolution of 8.1 × 8.1 km, addressing the challenges posed by the "gray zone" where the resolution is too coarse for explicit convection and too fine for traditional parameterizations. The goal is to identify the cumulus schemes that best capture rainfall dynamics in Thailand's tropical climate. Second, to evaluate the combined performance of SBU-YLin microphysics schemes and selected cumulus schemes across three nested domains: Domain 1 (8.1 × 8.1 km resolution), Domain 2 (2.7 × 2.7 km), and Domain 3 (0.9 × 0.9 km), covering Thailand's complex geographic and climatic features.

## 2. Research Methodology

### 2.1. Study area

Thailand is located between the latitudes 5°37' N and 20°27' N and longitudes 97°22' E and 105°37' E. It has a tropical climate, warm almost all year round, but from March through May, April is the hottest month, with an average temperature of 30°C (86°F), and it experiences three distinct seasons [3]. The observation data from 128 Thai Meteorological Department (TMD) stations are used as a reference dataset, as shown in Figure 1(a).

The simulations conducted in this study have a forecast lead time of 3 days from September 21 to 23, 2024. Typical synoptic and mesoscale meteorological conditions during the late monsoon season over Thailand, that is, convective rainfall, were chosen for this period. The hindcast was generated using a dynamical model initialized with the most recent available observations before the hindcast period. The model was run hourly, and outputs were validated against data from 128 TMD stations. The hindcast was initialized with the latest available observational data, ran hourly, and had detailed temporal resolution at each forecast hour. Because the forecast lead time is included in the simulation, the simulation output was validated against the observational data from 128 TMD stations.

### 2.2. WRF setup and configuration

The WRF model version 3.4.1 is configured for high-resolution rainfall forecasting over Thailand. The simulation uses three nested domains to balance large-scale dynamics and localized details, as shown in Figure 1(b). To evaluate cumulus parameterization schemes at a grid resolution of 8.1 × 8.1 km and address the challenges posed by the "gray zone," all cumulus schemes, as discussed in Table 1, are assessed following a comprehensive analysis of each scheme.

The WRF model was configured again to achieve the second objective (Table 2). This multi-domain nesting technique provides a scalable approach to model mesoscale and microscale meteorological features.

An 8.1 × 8.1 km resolution was chosen for the microphysics scheme experiment to be consistent with previous high-resolution numerical weather prediction studies over Thailand [16]. The SBU-YLin microphysics scheme, as implemented in all three domains following the approach by Wongwises et al. (2017), was selected due to its demonstrated suitability for high-resolution numerical weather prediction in this region [16].

It can effectively represent cloud and rainfall processes, which is critical for accurate predictions [16]. Convection is parameterized using a cumulus scheme (Tiedtke scheme) in the outermost domain (d01), enabling the model to resolve large-scale convective activity. Higher-resolution domains (d02 and d03) simulate convection, bypassing the need for cumulus parameterization [16]. This hierarchical modeling approach optimizes computational efficiency while maintaining high-resolution accuracy.

The Rapid Radiative Transfer Model for General Circulation Models (RRTMG) scheme oversees both longwave and shortwave radiation across all domains through its evaluation of $Q_c$ (cloud water), $Q_i$ (ice), and $Q_s$ (snow) hydrometeors. Numerous interactions between clouds and radiation are vital in maintaining

**Figure 1**
**Distribution of simulated areas and weather stations. (b) Nested domains for model configuration**

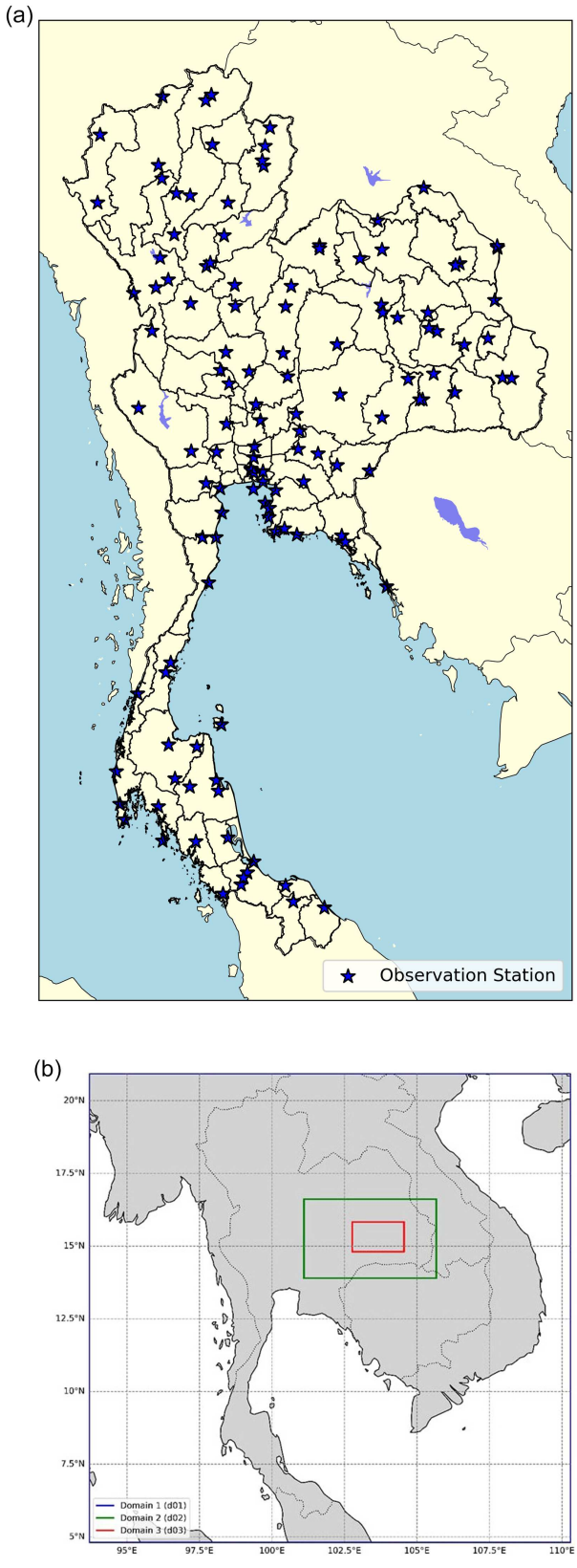


accurate cloud-radiation feedback during numerical weather prediction. The model also adopts the Mellor–Yamada–Janjic (MYJ) planetary boundary layer (PBL) scheme for boundary layer turbulence, ensuring robust coupling with surface-layer physics. The MYJ scheme is complemented by the Eta similarity surface layer and the Noah land surface model, which collectively enhance the representation of soil, vegetation, and hydrological processes critical to atmospheric feedback mechanisms [26].

The simulation uses a radiation time step of 15 s to enable the update of radiative processes frequently enough to capture rapid changes in the atmosphere. Other physics processes, such as the PBL and land surface models, are also synchronized in the temporal domain to enhance the accuracy and stability of the simulations. The selection of advanced microphysics schemes and high temporal resolution enhances the framework for the rainfall forecast in complex geographical and climatological conditions. This detailed configuration establishes a strong approach to high-resolution rainfall modeling.

## 2.3. KNN interpolation from the grid-to-point data

In this study, the K-Nearest Neighbors (KNN) algorithm was used for spatial interpolation to map total rainfall data from the WRF model grid to specific observation points based on their latitude and longitude coordinates [27] (Figure 2). KNN is a non-parametric regression technique that predicts the target value by averaging the outcomes of the nearest neighbors in the feature space (latitude and longitude in this case) [27]. The model was trained using a dataset of WRF grid points, where the total rainfall values were mapped to their respective geographic locations. The model was configured with 5 neighbors ($k = 5$) and distance-based weighting, assigning greater influence on nearer grid points predicting rainfall at observation locations. However, in complex topographic regions, steep terrain can cause abrupt variations in rainfall over short distances.

This selection aimed to make a balance between local accuracy and generalization, as spatial data exhibit nonlinear correlations between places and the measured variable (rainfall). To assess the sensitivity of interpolation results to the number of neighbors, a series of additional tests was conducted using different values of $k$ (between 3 and 10). These findings revealed that changes in $k$ in this range only caused minor changes in the interpolated rainfall fields, indicating that KNN interpolation is quite resistant to changes in k in this case. Smaller values of k were, however, chosen, resulting in local noise in regions with low grid coverage, whereas larger values of k (e.g., $k > 10$) were inclined to smooth rainfall gradients, especially where topography is complex. Thus, $k = 5$ was selected as a reasonable compromise between spatial smoothness and the maintenance of local variability of rainfall.

The interpolated rainfall values were obtained, and a bias correction procedure was then applied to WRF rainfall estimates to match them to observed rainfall data. The correction was done hourly by computing the difference between the predicted and observed rainfall at each observation point. The model's systematic bias was categorized into "Underestimation" or "Overestimation." An adjustment factor was then calculated and applied to improve the WRF rainfall estimates.

The corrections were made for up to 72 h, corresponding to the short-term forecasting periods of interest for operational meteorology. At each time step, the model was made responsive to changing atmospheric conditions by dynamically updating the adjustment factors. The correction approach presented here improves the reliability of WRF rainfall outputs, especially

**Table 1**
**Integrated description and performance evaluation of cumulus parameterization schemes used in the assessment. It summarizes each scheme's physical characteristics, parameterization options, and statistical performance metrics (bias, MAE, RMSE, Pearson's *r*, and $R^2$) from the ETS analysis**

| CumulusScheme | Choice | Notationin study | Moisturetendencies | Momentum tendencies | Shallowconvection | Radiation interaction | Description | Source | Bias | MAE | RMSE | *r* | $R^2$ |
|---|---|---|---|---|---|---|---|---|---|---|---|---|---|
| No cumulus scheme | – | RAIN-0 | – | – | – | – | – | – | –0.43 | 13.54 | 20.35 | 0.278 | –0.54 |
| Kain–Fritsch (KF) | 1 | RAIN-1 | $Q_c$, $Q_r$, $Q_i$, $Q_s$ | No | Yes | Yes | Deep and shallow convection sub-grid scheme using mass-flux approach with downdrafts and CAPE-removal time scale. | [28] | 8.90 | 18.20 | 24.95 | 0.24 | –1.32 |
| Betts–Miller–Janjic (BMJ) | 2 | RAIN-2 | N/A | No | Yes | No | Operational Eta column-moist adjustment scheme relaxing toward a well-mixed profile. | [29] | 0.38 | 11.71 | 17.83 | 0.29 | –0.18 |
| Grell–Freitas (GF) | 3 | RAIN-3 | $Q_c$, $Q_i$ | No | Yes | Yes | An improved GD scheme is designed to facilitate a smooth transition to cloud-resolving scales. | [30] | 5.92 | 16.35 | 24.44 | 0.24 | –1.22 |
| Grell-3 (G3) | 5 | RAIN-5 | $Q_c$, $Q_i$ | No | Yes | Yes | Enhanced GD version suitable for high-resolution use. | [31] | 8.40 | 17.24 | 26.70 | 0.24 | –1.66 |
| Tiedtke scheme | 6 | RAIN-6 | $Q_c$, $Q_i$ | Yes | Yes | No | Mass-flux type with CAPE-removal time scale, shallow part, and momentum transport. | [32] | –0.34 | 12.37 | 18.63 | 0.34 | –0.29 |
| Zhang–McFarlane | 7 | RAIN-7 | $Q_c$, $Q_i$ | Yes | Yes | Yes (RRTMG) | Community Earth System Model (CESM)-based mass-flux CAPE-removal scheme with momentum transport. | [33] | 5.23 | 13.60 | 17.94 | 0.33 | –0.20 |
| KF-CuP | 10 | RAIN-10 | $Q_c$, $Q_i$ | No | Yes | Yes | KF scheme modified with turbulence-linked trigger via boundary-layer PDFs. | [34] | 9.40 | 18.53 | 26.98 | 0.30 | –1.71 |

(*Continued*)

**Table 1**
(*Continued*)

| Cumulus Scheme | Choice | Notation in study | Moisture tendencies | Momentum tendencies | Shallow convection | Radiation interaction | Description | Source | Bias | MAE | RMSE | $r$ | $R^2$ |
|---|---|---|---|---|---|---|---|---|---|---|---|---|---|
| Multi-scale Kain–Fritsch | 11 | RAIN-11 | $Q_c$, $Q_r$, $Q_i$, $Q_s$ | No | Yes | Optional | Scale-dependent adjustment timescale and Low Cloud Cover (LCC)-based entrainment including convective momentum transport. | [35, 36] | –1.76 | 12.01 | 17.66 | 0.32 | –0.16 |
| KIAPS SAS | 14 | RAIN-14 | $Q_c$, $Q_i$ | Yes | Use shcu_physics = 4 | Yes (GFDL) | NSAS-based, scale-aware scheme. | [37, 38] | 1.22 | 11.62 | 16.56 | 0.29 | –0.02 |
| New Tiedtke | 16 | RAIN-16 | $Q_c$, $Q_i$ | Yes | Yes | No | Variant of Tiedtke used in REGCM4 and ECMWF cy40r1. | [32] | 0.17 | 10.02 | 12.27 | 0.29 | –0.12 |
| Grell–Dévényi (GD) | 93 | RAIN-93 | $Q_c$, $Q_i$ | No | No | Yes | Ensemble multi-closure, multi-parameter method with 144 sub-grid members. | [31] | 6.53 | 16.65 | 23.35 | 0.23 | –1.03 |
| New Simplified Arakawa–Schubert (NSAS) | 96 | RAIN-96 | $Q_c$, $Q_i$ | Yes | Optional | Yes (GFDL) | New mass-flux scheme with deep + shallow components and momentum transport. | [38] | 0.30 | 12.98 | 17.34 | 0.23 | –0.12 |
| Old Kain–Fritsch | 99 | RAIN-99 | $Q_c$, $Q_r$, $Q_i$, $Q_s$ | No | No | No | Deep convection scheme using mass flux with downdrafts and CAPE-removal time scale. | [38] | 2.42 | 12.44 | 17.48 | 0.27 | –0.14 |

**Note:** $Q_c$ = Cloud water, $Q_r$ = Rainwater $Q_i$ = Cloud ice, $Q_s$ = Snow.

**Table 2**
**WRF one-way nested model configuration parameters**

| Model setup | Configuration details |
|---|---|
| WRF model version | WRF 3.4.1 |
| Domain 1 (d01) | Grid points: 229 × 229; resolution: 8.1 × 8.1 km; longitude: 93.69436°E–110.30564°E; latitude: 4.80172°N–20.93652°N |
| Domain 2 (d02) | Grid points: 117 × 189; resolution: 2.7 × 2.7 km; longitude: 101.10143°E–105.66711°E; latitude: 13.89752°N–16.61506°N |
| Domain 3 (d03) | Grid points: 132 × 222; resolution: 0.9 × 0.9 km; longitude: 102.76904°E–104.55808°E; latitude: 14.80724°N–15.83002°N |
| Microphysics schemes | SBU-YLin (all domains) |
| Cumulus schemes | Domain 1: Tiedtke scheme; Domain 2: not used; Domain 3: not used |
| Longwave radiation | Scheme: RRTMG (all domains) interaction with $Q_c$, $Q_r$, $Q_i$, $Q_s$ |
| Shortwave radiation | Scheme: RRTMG (all domains) interaction with $Q_c$, $Q_r$, $Q_i$, $Q_s$ |
| PBL scheme | Scheme: MYJ (all domains) works with sfclay option 2; prognostic variables: TKE_PBL, EL_PBL |
| Surface layer scheme | Eta similarity (all domains) |
| Land surface model | Noah (all domains) |
| Radiation time step | 15 s (all domains) |
| PBL and land surface time step | 0 s (all domains) |

**Figure 2**
**KNN interpolation model flow diagram from the WRF grid to point data**

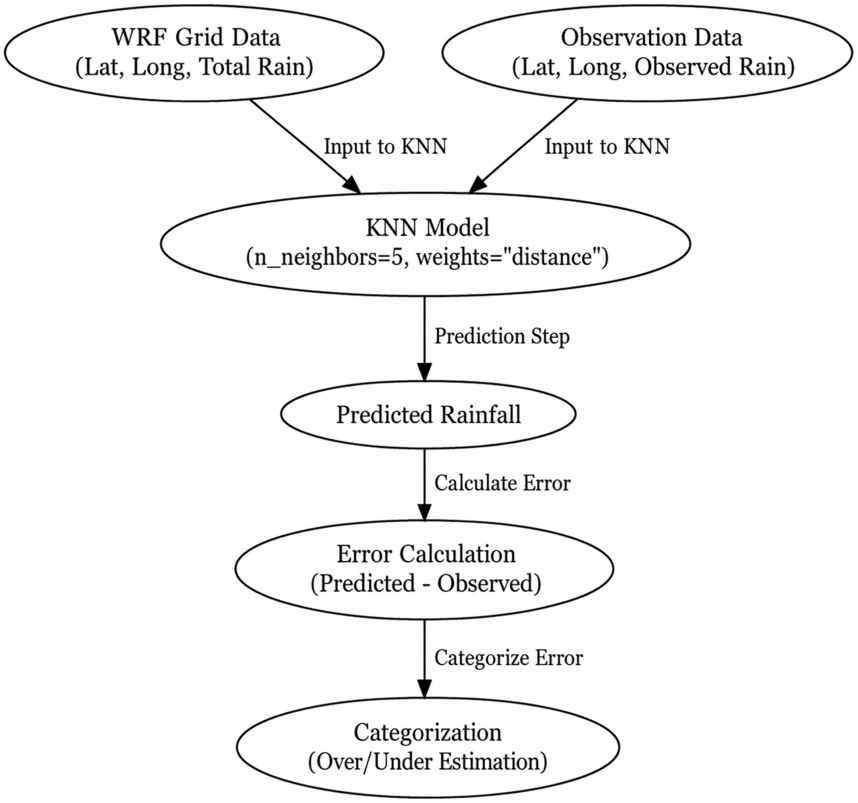


for high-resolution applications where accurate precipitation estimates are important.

## 2.4. Verification method

To assess the accuracy and reliability of the models, we used different forecast verification measures and compared the simulation results with the observed data (Table 3). Observation data from 128 TMD stations (Table S1) were interpolated by the KNN method to match the WRF model output. Statistical measures, including *r*, mean absolute error (MAE), false alarm ratio (FAR), Hit Score (HS), and root mean square error (RMSE), were used. Also, FAR and HS results in Figure S2 are given for the verification [4].

**Table 3**
**Description of verification metrics**

| Metrics | Description |
|---|---|
| $\text{FAR} = \frac{\text{FA}}{\text{FA} + \text{Hits}}$ | Forecast errors were measured using the FAR and HS [1] |
| $\text{RMSE} = \frac{\sqrt{\sum_{i=1}^{N}(\text{Pobs} - \text{Ppre})^2}}{N}$ | The nominal value of RMSE indicates a good model |
| $\text{MAE} = \sum \frac{(P_{pre} - P_{obs})}{N}$ | The MAE, the mean of the absolute differences between observed and predicted values divided by the number of observations, is also a critical metric for evaluating model performance |
| $r = \frac{n(\sum P_{obs} \times P_{pre}) - (\sum P_{obs})(\sum P_{pre})}{\sqrt{[n\sum P_{obs}^2 - (\sum P_{pre}^2)][n\sum P_{pre}^2 - (\sum P_{pre}^2)]}}$ | The $r$, which ranges from –1.00 to +1.00, measures the strength and direction of a linear relationship between two variables [4] |

## 3. Results and Discussion

In this section, cumulus parameterization schemes, along with the SBU-YLin microphysics scheme, are thoroughly assessed. The evaluation is for a 3-day rainfall prediction over three nested domains from September 20 to 23, 2024. Rainfall intensity is analyzed according to the TMD classification as presented in Table 4.

**Table 4**
**TMD's different rainfall categories**

| Rainfall category | Rainfall range (mm) |
|---|---|
| Trace | 0.0–0.1 |
| Light rain | 0.1–10.0 |
| Moderate rain | 10.1–35.0 |
| Heavy rain | 35.1–90.0 |
| Very heavy rain | ≥ 90.0 |

### 3.1. Assessment of cumulus parameterization schemes

A comparative analysis of several cumulus schemes in the WRF model (Table 1) is made to assess the efficacy of the schemes in simulating rainfall events over Thailand under the domain 8.1 x 8.1 km on September 20, 2024. Figure S1(a)–(n) shows the performance of these schemes using grid-to-point data interpolation using the KNN method and standard deviation (SD) and mean values of rainfall underestimation and overestimation. The performance skill values presented correspond to the total forecast duration of 24 h.

Figure S1(a) shows the weakest performance of the control configuration without cumulus parameterization (RAIN-0). The rainfall estimation is equally underestimated (52.34% underestimation, 47.66% overestimation) and overestimating (mean underestimation of −13.25 mm, SD = 14.74 mm; mean overestimation of 13.88 mm, SD = 15.93 mm). The significant variability in rainfall estimates shows that omitting cumulus parameterization produces significant inconsistencies in simulated precipitation patterns.

RAIN-1 reduces underestimation to 34.38% and overestimation to 65.63% (Figure S1(b)). Despite its ability to improve rainfall simulation, it introduces a strong overestimation bias (mean overestimation: 20.75 mm, SD = 17.65 mm) resulting from an overprediction of heavy rainfall events. Similarly, the RAIN-2 reduces underestimation to 44.53% and increases overestimation to 55.47% (Figure S1(c)). Still, it is not applicable for operational forecasting with a higher variability (underestimation mean: −12.63 mm, SD = 17.06 mm).

However, the RAIN-3 and RAIN-5 schemes introduce even more overestimation tendencies with proportions of 60.16% and 71.88% (Figures S1(d)–(e)). The mean overestimation of the RAIN-3 scheme is 18.61 mm (SD = 19.90 mm), and the RAIN-5 scheme is 17.90 mm (SD = 21.08 mm). Although these schemes enhance the simulation of extreme rainfall events, their significant variability limits their reliability for operational use.

On the other hand, the RAIN-6 scheme exhibits a more balanced performance with underestimation and overestimation proportions of 42.19% and 57.81% (Figure S1(f)). The mean underestimation is −14.96 mm (SD = 17.33 mm), and the mean overestimation is 10.47 mm (SD = 10.61 mm), indicating moderate skill in rainfall representation. The RAIN-16 scheme further improves this balance by producing an equal amount of underestimation (50%) and overestimation (50%) with less variability (mean underestimation: −12.75 mm, SD = 15.23 mm; mean overestimation: 13.30 mm, SD = 10.02 mm) (Figure S1(k)). The results indicate that the Tiedtke schemes are practical for convective rainfall simulations in Thailand.

For high-intensity rainfall events, the RAIN-7 and RAIN-10 schemes (Figures S1(g)–(h)) exhibit strong overestimation tendencies (~67.97%) with considerable variability, rendering them inaccurate. This poor performance can be attributed to the simplified or inadequate representation of deep convection processes in these schemes, which leads to excessive convective rainfall generation. However, the multi-scale RAIN-11 scheme provides a more balanced distribution with 50.78% underestimation and 49.22% overestimation (Figure S1(i)) and a mean overestimation of 10.50 mm (SD = 10.15 mm). It implies that moderate to high rainfall events are forecasted more accurately.

Moderate performance is also shown by additional schemes, such as the RAIN-14 and RAIN-96, which overestimate proportions of 64.06% and 58.59%, respectively (Figures S1(j) and (m)). However, their biases in extreme rainfall events remain problematic despite reasonable spatial distribution. Like RAIN-1, the RAIN-99 scheme also shows overestimation tendencies (Figure S1(n)).

Further insight into scheme performance is given by a detailed evaluation across different rainfall categories (Table 1; Figures 3 and 4). In all categories, the control case (RAIN-0) performs the worst, especially for trace and light rainfall predictions ($r = -0.05$ and $r = -0.24$) and extreme overestimation errors (RMSE = 99.94 mm) in the heavy and very heavy rainfall events.

**Figure 3**
**Spatial comparison of observations from TMD stations vs WRF output over Thailand**

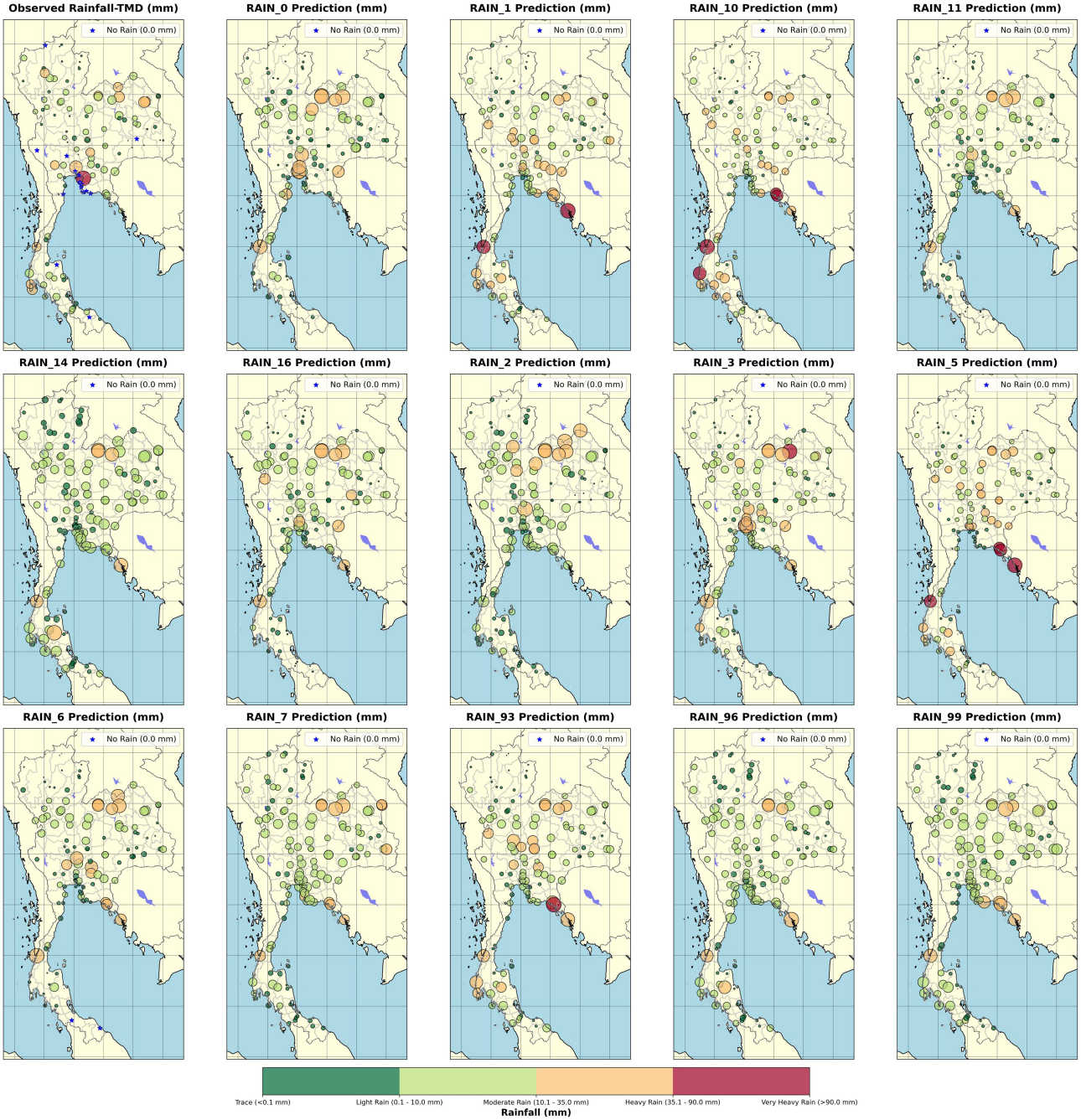


RAIN-1 and its derivatives—RAIN-10 and RAIN-11—are incremental improvements, and RAIN-11 is the most accurate. The *r* and error statistics of RAIN-11 are superior to those of the other schemes, especially for moderate and heavy rainfall, and it is a viable candidate for operational forecasting at all lead times.

The RAIN-6 and RAIN-16 are very stable in predicting heavy and very heavy rainfall events (i.e., >35.0 mm/day as per Table 4) and show a well-balanced distribution of underestimation and overestimation errors. Due to their reduced variability and improved spatial rainfall distribution, they are suitable for rainfall modeling in Thailand.

Further validation of the different cumulus parameterization schemes is performed by a spatial comparison of WRF model outputs with TMD observations for the different TMDs' rainfall intensity classification (Figures 3 and 4). The RAIN-6 is among the most suitable tested schemes, providing a balanced and reliable rainfall estimation in all six rainfall intensity categories. It has moderate biases, lower variability, and better spatial representation, which makes it a potential improvement in WRF model performance in convective rainfall simulations of Thailand.

The evaluation of the cumulus parameterization schemes shows the importance of choosing the appropriate scheme to

**Figure 4**

**Comparison of predicted rainfall under various cumulus parameterization schemes as per the TMD's rainfall intensity classification**

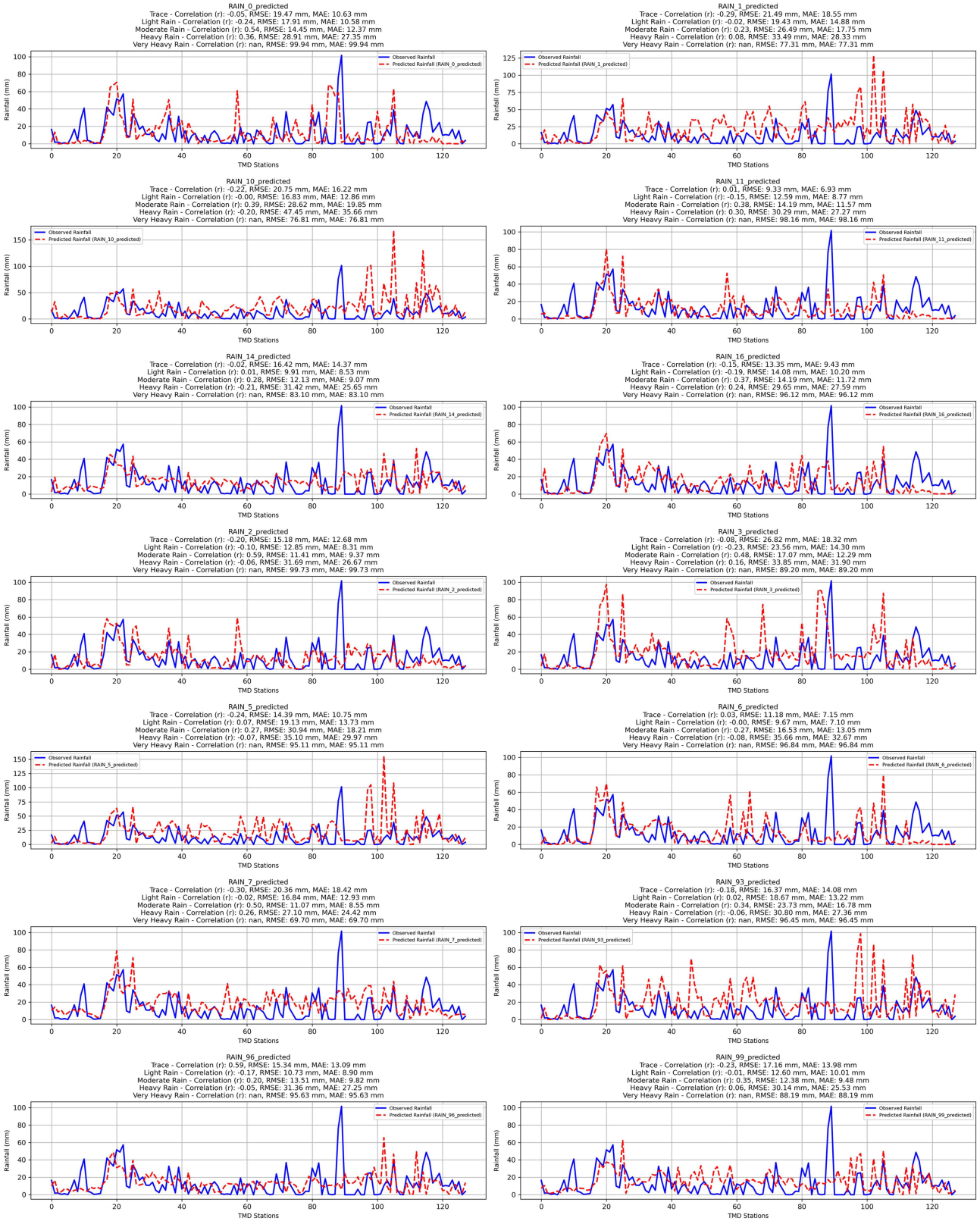

improve the accuracy of rainfall prediction in WRF simulations. Including a suitable cumulus scheme is necessary to prevent severe underestimation and overestimation inconsistencies when cumulus parameterization (RAIN-0) is omitted. Despite slight improvements in rainfall representation, the RAIN-1 and RAIN-11 schemes struggle with high overestimation biases. RAIN-16 is the most stable and reliable scheme among the Tiedtke schemes and, hence, is the best option for operational rainfall forecasting in Thailand.

### 3.2. Evaluation of the combined performance of SBU-YLin and RAIN-16 cumulus schemes across nested domains

In this section, the integrated performance of the SBU-YLin microphysics scheme and RAIN-16 cumulus parameterization scheme is examined in terms of their performance in the three nested domains (Domain 1: 8.1 × 8.1 km resolution, Figures 5 and 6; Domain 2: 2.7 × 2.7 km, Figures 7 and 8; Domain 3:

**Figure 5**
**Spatial comparison of observations from TMD stations vs WRF output over Domain 1: (a) comparison for Day 1, (b) comparison for Day 2, and (c) comparison for Day 3**

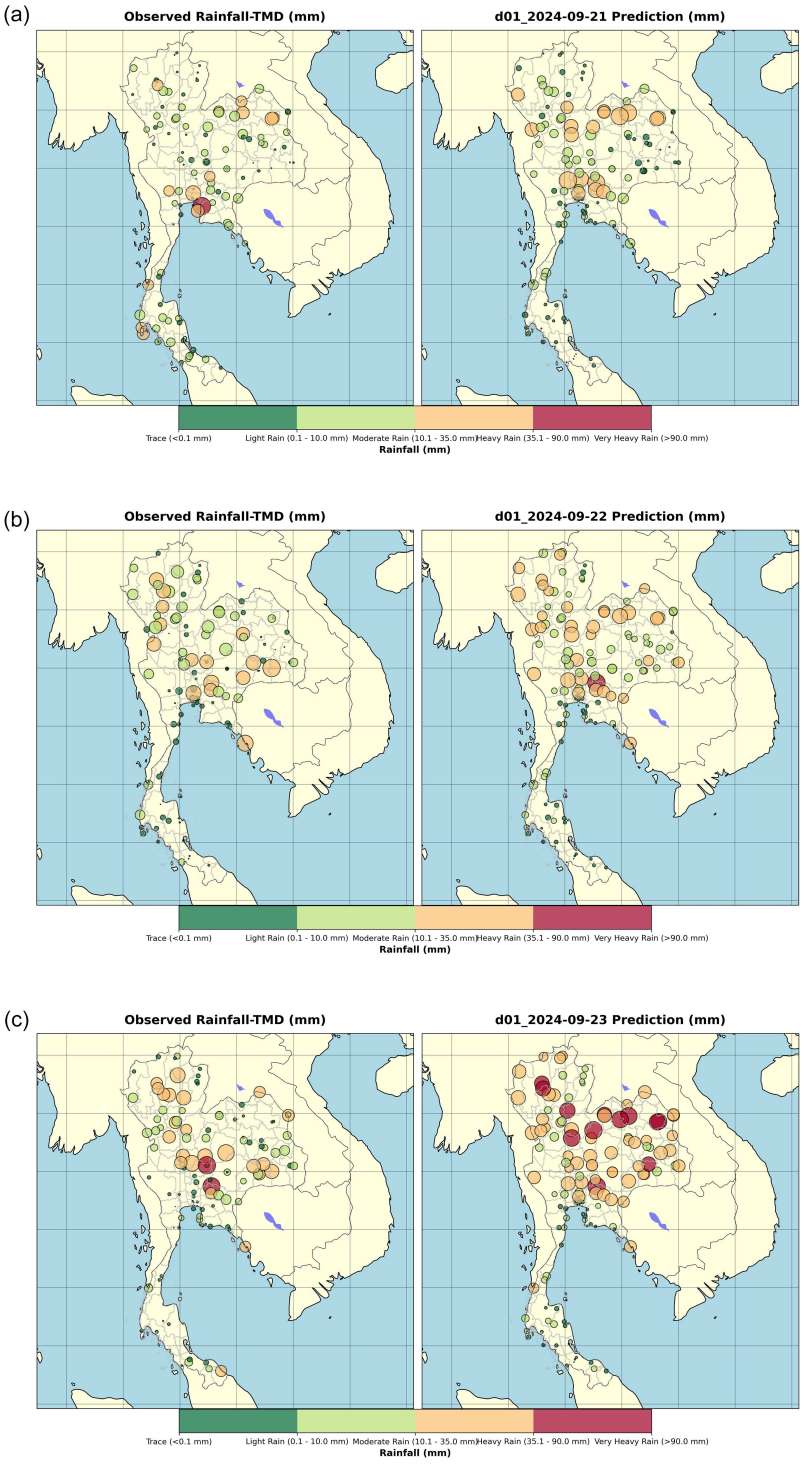

**Figure 6**
**Comparison of predicted rainfall under TMD's rainfall intensity classification for Domain 1: (a) comparison for Day 1, (b) comparison for Day 2, and (c) comparison for Day 3**

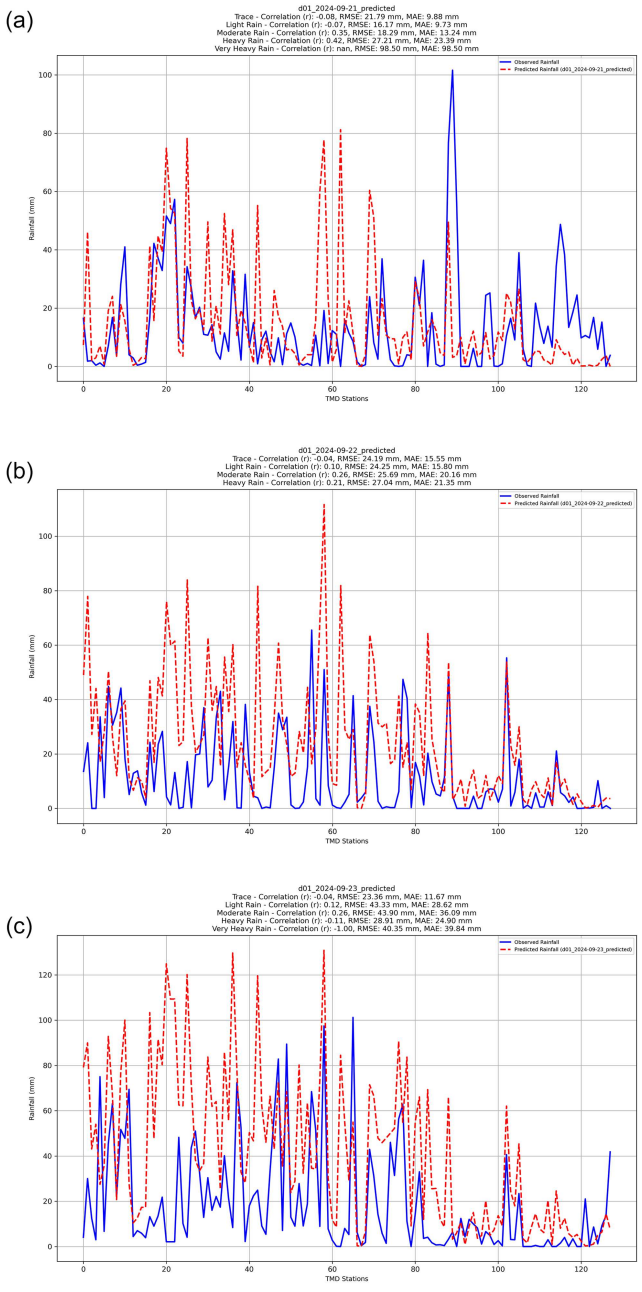


0.9 × 0.9 km, Figures 9 and 10). These domains are intended to capture Thailand's varied geographic and climatic conditions to enable multi-scale evaluation of rainfall prediction accuracy.

### *3.2.1. Domain 1 (8.1 × 8.1 km resolution)*

For Day 1, the results of the WRF model for Domain 01 (8.1 × 8.1 km) on September 21, 2024, are presented in Figures 5(a), 6(a), and S3(a). The mean rainfall observed was 13.64 mm with an SD of 16.68 mm, while the predicted mean was 15.54 mm with an SD of 18.85 mm, which shows that the model overestimated the mean rainfall by 55.38% (see Figure S3(a)). This difference raises questions about the model's microphysics schemes' biases in simulating sub-grid scale processes such as cloud formation and rainfall initiation. The correlation analysis reveals that moderate and heavy rainfall events have positive correlations $r$ of 0.35 and 0.42, respectively, indicating that the model has higher accuracy in simulating high-intensity rainfall. Nevertheless, trace and light rainfall reveal negative coefficients (−0.08 and −0.07), which are suggestive of mismatches that are due to the inability of the model to simulate low-intensity rainfall adequately, which can be attributed to inadequate grid resolution and difficulties in the formulation of rain processes. The RMSE increases from 27.21 mm for heavy rain to 98.50 mm for very heavy rain, showing that model errors increase with increasing rainfall intensity (see Figure 6(a)).

For Day 2 (September 22, 2024), the results of the WRF model's rainfall predictions for Domain 1 are presented in Figures 5(b), 6(b), and S3(b). The observed mean rainfall of 11.73 mm, with an SD of 14.90 mm, is lower than the predicted mean of 25.36 mm and an SD of 22.83 mm, resulting in an overestimated 79.23% (see Figure S3(b)). The $r$ between observed and predicted rainfall categories is low for both trace rain (−0.04) and light rain (0.10), suggesting low model efficiency. A minor enhancement is observed for moderate (0.26) and heavy (0.21) rainfall, but these correlations are still inadequate for operational forecast application (see Figure 6(b)). The RMSE for different rain categories has been increasing with the increase in rain intensity, ranging from 24.19 mm for trace rain to 27.04 mm for heavy rain, along with high MAE.

For Day 3 (September 23, 2024), the results are shown in Figures 5(c), 6(c), and S3(c). The observed mean rainfall is 18.74 mm (SD = 23.22 mm), while the predicted mean is 41.94 mm (SD = 34.20 mm); hence, the overestimation of 81.54 % is much higher than the underestimation of 18.46% (see Figure S3(c)). It indicates excessive convective activity or errors in the representation of mesoscale dynamics within the model's rainfall schemes. Correlation analysis reveals that the model performs poorly for trace and light rainfall, with r of −0.04 and 0.12, respectively, indicating challenges in simulating low-intensity events. Moderate rain has a slightly better relationship of 0.26, heavy rainfall has a poor relationship of −0.11, and very heavy rain has a severely out-of-phase relationship of −1.00. The values of RMSE and MAE for intense rainfall were greater than 43.90 mm and 36 mm, respectively, indicating the models' inability to simulate extreme rainfall (see Figure 6(c)).

### *3.2.2. Domain 2 (2.7 × 2.7 km)*

For Domain 2, the results for Day 1 (September 21, 2024) are presented in Figures 7(a), 8(a), and S4(a), where the WRF model was biased to overestimate the rainfall with a mean of 13.34 mm against the observed mean of 9.80 mm. The higher SD of the predictions (20.39 mm) compared to that of the observations (9.53 mm) shows that the model overestimates spatial variability (see Figure 8(a)). The fact that overestimation was the most common type of systematic bias, with 53.57% of predictions, only strengthens the conclusion (see Figure S4(a)). The model gives a reasonable workout for light rain events with an $r$ of 0.463 but fails for moderate rainfall with an $r$ of 0.437, RMSE of 25.67 mm, and MAE of 16.59 mm. These statistics indicate that the model is not accurate for moderate rainfall and overestimates the intensity of observed rainfall. The fact that no models can predict 0% means that the model cannot mimic the observed rainfall distribution.

For Day 2 (September 22, 2024), the results are shown in Figures 7(b), 8(b), and S4(b). The model still overestimates the rainfall with a mean of 26.89 mm, while the observed mean is

**Figure 7**
**Spatial comparison of observations from TMD stations vs WRF output over Domain 2: (a) comparison for Day 1, (b) comparison for Day 2, and (c) comparison for Day 3**

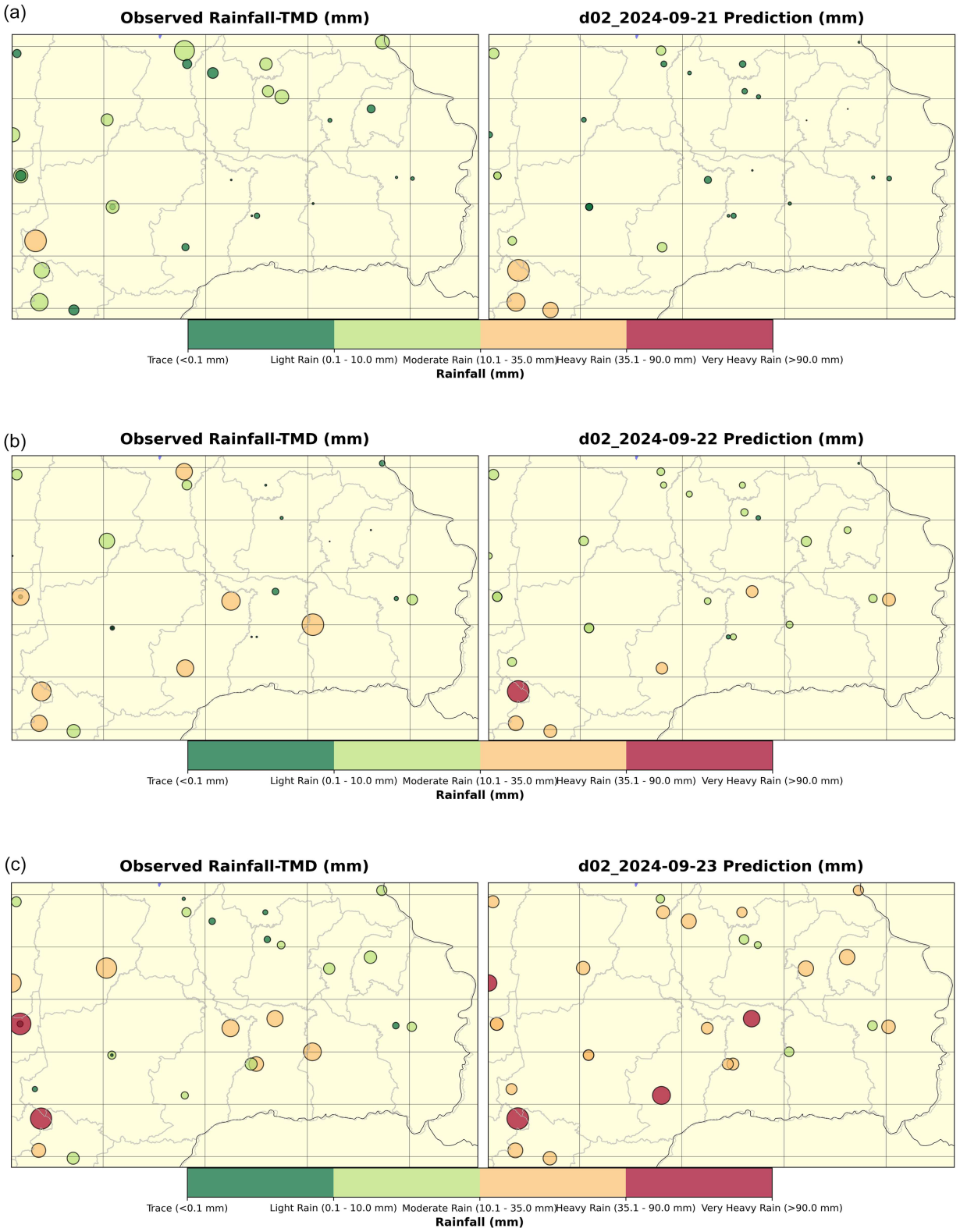

**Figure 8**
**Comparison of predicted rainfall under TMD's rainfall intensity classification for Domain 2: (a) comparison for Day 1, (b) comparison for Day 2, and (c) comparison for Day 3**

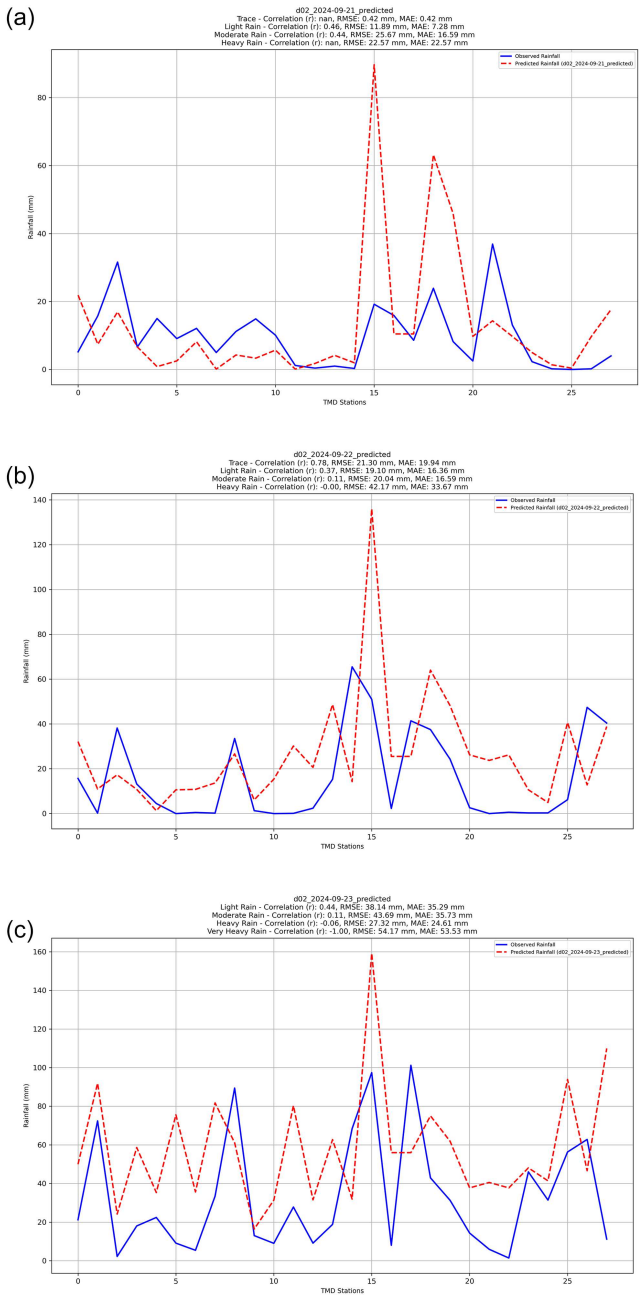


15.89 mm. The predicted rainfall variability in SD (26.01 mm) is still quite close to the observed values (19.93 mm), and there seems to be some enhancement in capturing the spatial distribution. However, overestimation prevails (71.43%), and correlations for the higher rainfall categories are much lower. For moderate rainfall, the coefficient is 0.11, while for heavy rainfall, it is slightly negative (−0.004), suggesting poor model performance during intense events. RMSE and MAE for the heavy rainfall (42.17 mm and 33.67 mm) indicate that the model poorly predicts extreme events. The high $r$ values for trace rainfall (0.78) indicate a bias toward low rainfall, while the model overestimates heavy rainfall.

For Day 3 (September 23, 2024), the results are shown in Figures 7(c), 8(c), and S4(c). The overestimation of rainfall intensifies, with the predicted mean of 58.28 mm compared to the observed mean of 33.20 mm. The predicted SD (30.29 mm) is slightly more than the observed variability (29.94 mm); hence, the extremes are overestimated. Overestimation prevails in predictions (85.71%), and the $r$ for heavy rainfall (−0.059) and very heavy rainfall (−1.000) indicates that the model performs poorly for intense events. The RMSE and MAE are notably high for very heavy rain (54.17 mm and 53.53 mm, respectively), which further supports the conclusion that the models struggle to predict heavy and very heavy rainfall. As with other models, the model performs well in simulating broad spatial rainfall patterns for lighter rain events but poorly for heavier events, particularly those associated with convective processes. The lack of 0% also underlines the inability of the model to simulate the observed rainfall characteristics for Day 3.

### *3.2.3. Domain 3 (0.9 × 0.9 km)*

The rainfall comparison for Day 1 (September 21, 2024) is shown in Figures 9(a), 10(a), and S5(a), which showed a mean of 2.35 mm and an SD of 3.26 mm, higher than the observed mean of 0.70 mm and SD of 0.89 mm. It indicates a strong overestimation bias, with 83.33% of predictions falling into the overestimation category and no instances of perfect estimation. The RMSE of 3.87 mm and MAE of 2.35 mm highlight significant discrepancies in capturing traces. Correlation analysis suggests a weak or negligible relationship.

For Day 2 (September 22, 2024), rainfall predictions exhibited a mean of 16.16 mm and an SD of 12.56 mm, which was lower than the observed mean of 19.97 mm but showed reduced variability (observed SD: 28.93 mm) (see Figures 9(b), 10(b), and S5(b)). The overestimation bias persisted, with 66.67% of predictions classified as overestimated and 33.33% underestimated. Correlation analysis revealed moderate alignment for light rain ($r$ = 0.68) but inconsistent performance for heavier rainfall categories, suggesting mixed prediction reliability across rainfall intensities. The RMSE of 28.20 mm and MAE of 20.42 mm indicate substantial errors in higher-intensity events. The finer prediction variability suggests that the model does not fully capture the dynamic range of observed rainfall. These findings indicate challenges in achieving a balanced representation of rain, especially under conditions of moderate-to-heavy rainfall.

On Day 3 (September 23, 2024), predictions produced a mean rainfall of 55.11 mm and an SD of 22.64 mm, exceeding the observed mean of 48.78 mm and 16.66 mm (see Figures 9(c), 10(c), and S5(c)). The overestimation bias remained dominant (66.67%), with 33.33% classified as underestimation. $r$ revealed an inverse relationship for moderate ($r$ = −1.00) and heavy rain ($r$ = −0.39), indicating systematic misrepresentation of rainfall distribution across these categories. Figure 10 highlights the significant prediction errors, with an RMSE of 37.68 mm and an MAE of 32.39 mm.

This research evaluated the WRF model cumulus and microphysics parameterization schemes for Thailand's tropical climate using a systematic assessment. Selected schemes demonstrated the best performance, controlling underestimations and overestimations during different rainfall intensity conditions. These schemes demonstrate performance levels that make them viable for operational weather prediction applications. The model behavior underwent multi-scale evaluation through the implementation of nested domains. The 8.1 × 8.1 km Domain 1 area showed

**Figure 9**
**Spatial comparison of observations from TMD stations vs WRF output over Domain 3: (a) comparison for Day 1, (b) comparison for Day 2, and (c) comparison for Day 3**

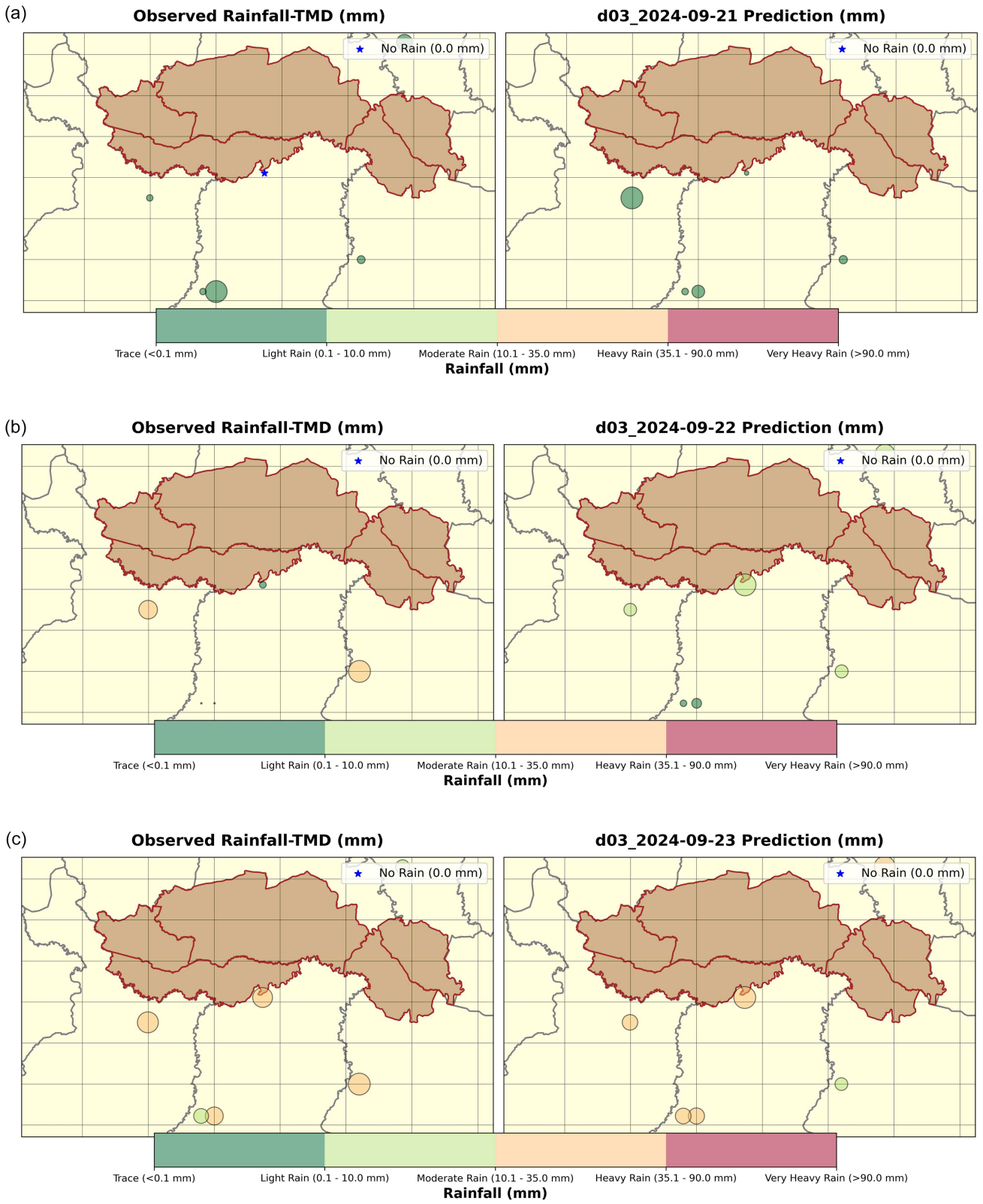

**Figure 10**
**Comparison of predicted rainfall under TMD's rainfall intensity classification for Domain 3: (a) comparison for Day 1, (b) comparison for Day 2, and (c) comparison for Day 3**

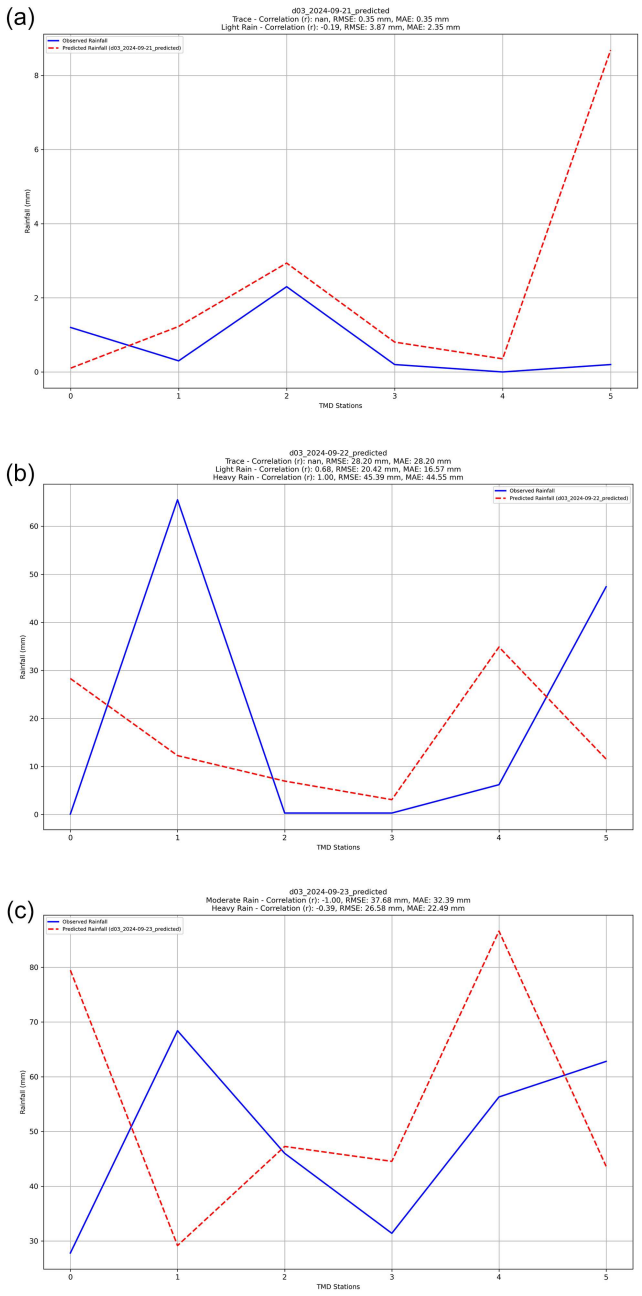


considerable errors in rainfall intensity measurement, and its RMSE increased proportionally to precipitation levels. The bias characteristics from Domain 2 remained consistent while achieving better spatial accuracy. The Domain 3 area faced significant difficulties due to a growing tendency to mispredict intense rainfall events.

The spatial pattern of rainfall showed topographical effects because elevated areas received increased precipitation through orographic lifting processes. The performance of cumulus schemes showed a direct relationship with topographical complexity, as triggering mechanisms tended to overestimate rainfall in mountainous areas. These discrepancies in rainfall estimation stem from the model's representation of terrain-induced convection.

Similarly, Kaewmesri et al. [16] demonstrated that SBU-YLin outperformed other methods in terms of RMSE and MAE results, a finding that this study also confirmed. The present research confirmed SBU-YLin's effectiveness in bias reduction for tropical rainfall modeling [16].

RAIN-1 demonstrates that the KF scheme produced excessive predictions when measuring heavy rainfall quantities. Musa et al. [14] evaluated cumulus schemes in Sudan's semi-arid region and determined that the BMJ scheme performed better for temperature prediction than rainfall prediction. The operational value RAIN-2 for rainfall prediction was restricted by its variable bias patterns in this research. The research findings demonstrate the extensive difficulties of using the BMJ scheme in rain regimes controlled by convection.

The research findings regarding RAIN-3 reveal performance constraints like those in previous studies, as it produces excessive rainfall estimates during storm events. Otieno et al. [10] examined KF and BMJ schemes in East Africa, where KF showed better stability in spatial rainfall distribution. Still, BMJ displayed high variability in extreme precipitation prediction [10]. The results from RAIN-1 in the current study validate previous findings by showing that KF produces an acceptable spatial distribution yet displays typical mass-flux-based scheme overestimation behavior. The study findings from different regions demonstrate that model-based cumulus parameterization errors exist independently of regional climate characteristics. The KF scheme consistently overestimates rainfall across various geographical locations, demonstrating its sensitivity to intense precipitation events.

Amirudin et al. [6] demonstrated that Tiedtke represents an optimal choice for monsoon rainfall simulation in SEA regions. Research findings match the results, showing that RAIN-6 and its updated version operate effectively with minimal variation, strengthening their operational potential [6]. Merino et al. [18] demonstrated that Morrison and Thompson schemes enhance convective system predictability. The research results validate the findings, as SBU-YLin achieved better predictions, albeit at the cost of greater computational resources. Torsri et al. [15] assessed WRF cumulus and microphysics schemes for tropical cyclone simulations in Thailand. The researchers showed that combining Tiedtke and SBU-YLin advanced schemes produced superior model performance across all rainfall intensity levels [15]. These findings reinforce the reliability of these schemes for monsoon climates because they match the current study's results. The WRF model shows the potential to accurately simulate convective precipitation after achieving optimal configuration in regions that experience strong monsoonal influences.

Multi-domain nesting is a valuable methodological tool that helps researchers study mesoscale and microscale precipitation dynamics. The proposed framework proves valuable for Thailand because rainfall patterns result from monsoonal activity and mountain-related weather systems [15].

However, despite the high performance, there are certain limitations in scheme RAIN-16 in the sphere of applicability. The scheme is designed and tuned to convey active and wet tropical and monsoon conditions, which are convectively active. It implies that it may not parameterize deep convection or cloud microphysics so effectively in arid or mid-latitude latitudes, where the process of convective initiation is much different. Additionally, the parameter of the RAIN-16 scheme is sensitive to the local conditions of the boundary-layer and surface fluxes, so it may be required to carry out regional recalibration when applied outside the Southeast Asian monsoon area. These limitations imply

that even though RAIN-16 is highly suitable in Thailand and other tropical conditions, it should be utilized with caution when employed in more climatological or intercontinental simulations without any pertinent adjustment or retesting.

In addition to that, the physical and geographical form of Thailand is also a contributor to the development and success of the WRF model. Thailand has a complicated topography with high mountainous regions in the north and low floodplains in the central basin that form powerful orographic lifting and mesoscale convective systems that interact very intensively with monsoonal flows. These properties demand the design of the domain, the tuning of terrain resolution, and parameterization to ensure that the convective processes are realistically represented. Further, the land-sea gradient across the GoT (Gulf of Thailand) and Andaman Sea introduces high diurnal convectional variability; that is, the model calibration at the coastal and inland regions should be done based on the thermodynamic conditions, which are spatially varying. Therefore, RAIN-16 and other plans cannot be accurately interpreted in relation to Thailand's climatic and topographical conditions.

The evaluation results show that all parameterization schemes tend to produce overestimated extreme rainfall amounts, indicating ongoing difficulties in representing convective processes. Weak $r$ values for extreme events emerged as the main challenge in Domain 3, as they made it difficult to resolve small-scale convective systems at high spatial resolution. Additionally, the "gray zone" resolution range (3–10 km) presents a fundamental challenge, as traditional cumulus schemes remain inadequate, while explicit convection modeling remains computationally prohibitive.

Future research should explore hybrid convection-permitting approaches and adaptive parameterization frameworks that can bridge this gray zone and further enhance RAIN-16's applicability to other tropical regions.

## 4. Conclusion

This study systematically evaluated cumulus and microphysics parameterization schemes in the WRF model to enhance rainfall prediction in Thailand's tropical climate. The RAIN-16 schemes were identified as the most suitable, achieving balanced underestimation and overestimation rates (approximately 50%) and reducing variability compared to other schemes, with mean underestimation and overestimation of −12.75 mm and 13.30 mm, respectively, for the RAIN-16. The RAIN-16 scheme demonstrated consistent stability across different rainfall categories, highlighting its operational viability under the SBU-YLin microphysics scheme, with notable reductions in RMSE and MAE, which support the accurate simulation of heavy rainfall. Nested domain analysis provided critical insights into scale-dependent model behavior. Domain 1 (8.1 × 8.1 km) exhibited significant overestimations of heavy rainfall events, with RMSE reaching 98.50 mm for very heavy rainfall. Domain 2 (2.7 × 2.7 km) improved spatial precision but retained systematic biases. In comparison, Domain 3 (0.9 × 0.9 km) faced challenges in simulating small-scale convection, with overestimation dominating 83.33% of predictions and RMSE exceeding 37.68 mm for intense events. Weak to insignificant $r$ for extreme rainfall categories (e.g., −1.00 for Domain 3) highlighted limitations in resolving mesoscale convective processes.

Evaluation of the SBU-YLin scheme across nested domains revealed significant challenges in simulating extreme rainfall events. Domain 1 (8.1 × 8.1 km) experienced substantial overestimation of heavy rainfall events, with RMSE reaching 98.50 mm. In contrast, Domain 3 (0.9 × 0.9 km) exhibited pronounced overestimation for localized convection, with RMSE exceeding 37.68 mm.

Nevertheless, the RAIN-16 scheme is to be viewed in relation to its climatological and geographical setting. It is parameterized to deep convective systems standard to the tropical monsoon regimen of Thailand and might not be equally effective in mid-latitude or dry cases. Regional recalibration of convective trigger parameters and moisture flux when used outside of Southeast Asia is required to ensure reliable predictions.

Thailand has regional peculiarities, such as high humidity, a high level of monsoonal influence, and complicated orography: these factors have a significant effect on the model behavior. Rainfall distribution and intensity are highly influenced by the presence of Orographic lifting in the highlands of the north and land-sea breeze interactions in the GoT and Andaman coast. Thus, to model these spatially heterogeneous atmospheric dynamics successfully, domain settings and physics selections are needed.

Although RAIN-16 has been observed to perform very well in convective rainfall modeling, its predictive capability decreases under high-resolution ranges where explicit convection takes over. This weakness highlights the difficulty of modeling in the so-called gray zone, where neither standard cumulus parameterizations nor fully resolved convection models are ideal.

## Recommendations

Future studies should focus on refining parameterization schemes to better capture high-intensity rainfall and small-scale convection processes. Additionally, integrating advanced observational datasets and ensemble-based modeling approaches could enhance the accuracy and reliability of rainfall forecasts.

Additionally, it is necessary to consider the computational cost of various cumulus and microphysics schemes in future research to determine their practicability. Such an analysis would allow better insight into the trade-off between predictive accuracy and computational efficiency.

## Funding Support

This research work was conducted under the auspices of King Mongkut's University of Technology Thonburi (KMUTT), Thailand Science, Research and Innovation (TSRI), and the NSRF Fiscal year 2024 Grant number FRB670016/0164. The Reinventing University Program 2025, under the Office of the Permanent Secretary, Ministry of Higher Education, Science, Research and Innovation, Thailand, also supported this work.

## Ethical Statement

This study does not contain any studies with human or animal subjects performed by any of the authors.

## Conflicts of Interest

The authors declare that they have no conflicts of interest to this work.

## Data Availability Statement

The data used in this study were obtained from TMD with permission and are not publicly available.

## Author Contribution Statement

**Usa Wannasingha Humphries:** Conceptualization, Methodology, Software, Formal analysis, Investigation, Resources, Writing – review & editing, Supervision, Project administration, Funding acquisition. **Muhammad Waqas:** Validation, Investigation, Data curation, Writing – original draft, Visualization. **Boonlert Archevarahuprok:** Conceptualization, Methodology, Software, Formal analysis, Investigation, Data curation. **Porntip Dechpichai:** Validation, Visualization. **Angkool Wangwongchai:** Conceptualization, Methodology, Software, Formal analysis, Writing – review & editing, Supervision, Project administration. **Boobphachard Chansawang:** Writing – review & editing, Visualization.

## References


[1] Waqas, M., Humphries, U. W., Hlaing, P. T., & Ahmad, S. (2024). Seasonal WaveNet-LSTM: A deep learning framework for precipitation forecasting with integrated large scale climate drivers. *Water*, *16*(22), 3194. https://doi.org/10.3390/w16223194

[2] Kochkov, D., Yuval, J., Langmore, I., Norgaard, P., Smith, J., Mooers, G., . . . , & Hoyer, S. (2024). Neural general circulation models for weather and climate. *Nature*, *632*(8027), 1060–1066. https://doi.org/10.1038/s41586-024-07744-y

[3] Waqas, M., Humphries, U. W., & Wangwongchai, A. (2025). Advances in atmospheric, oceanic, and coupled models for meteorological forecasting. *Natural Hazards Research*. Advance online publication. https://doi.org/10.1016/j.nhres.2025.10.003

[4] Waqas, M., Humphries, U. W., Hlaing, P. T., Wangwongchai, A., & Dechpichai, P. (2024). Advancements in daily precipitation forecasting: A deep dive into daily precipitation forecasting hybrid methods in the tropical climate of Thailand. *MethodsX*, *12*, 102757. https://doi.org/10.1016/j.mex.2024.102757

[5] Lin, J., Qian, T., Bechtold, P., Grell, G., Zhang, G. J., Zhu, P., . . . , & Han, J. (2022). Atmospheric convection. *Atmosphere-Ocean*, *60*(3-4), 422–476. https://doi.org/10.1080/07055900.2022.2082915

[6] Amirudin, A. A., Salimun, E., Zuhairi, M., Tangang, F., Juneng, L., Mohd, M. S. F., & Chung, J. X. (2022). The importance of cumulus parameterization and resolution in simulating rainfall over peninsular Malaysia. *Atmosphere*, *13*(10), 1557. https://doi.org/10.3390/atmos13101557

[7] Savazzi, A. C. M., Nuijens, L., de Rooy, W., Janssens, M., & Siebesma, A. P. (2024). Momentum transport in organized shallow cumulus convection. *Journal of the Atmospheric Sciences*, *81*(2), 279–296. https://doi.org/10.1175/JAS-D-23-0098.1

[8] Kan, Y., Liu, C., Liu, Y., & Zhou, C. (2015). Evaluation of WRF microphysics and cumulus parameterization schemes in simulating a heavy rainfall event over Yangtze River delta. In *Remote Sensing and Modeling of Ecosystems for Sustainability XI: Proceedings of SPIE*, *9610*, 96100R. https://doi.org/10.1117/12.2185766

[9] Jiang, J., & Wang, Y. (2025). The role of outflow-layer inertial stability in governing the radial location of secondary eyewall formation in tropical cyclones. *Journal of Geophysical Research: Atmospheres*, *130*(16), e2025JD043708. https://doi.org/10.1029/2025JD043708

[10] Otieno, G., Mutemi, J. N., Opijah, F. J., Ogallo, L. A., & Omondi, M. H. (2020). The sensitivity of rainfall characteristics to cumulus parameterization schemes from a WRF model. Part I: A case study over East Africa during wet years. *Pure and Applied Geophysics*, *177*(2), 1095–1110. https://doi.org/10.1007/s00024-019-02293-2

[11] Gui, S., Yang, R., Cao, J., & Huang, W. (2020). Precipitation over East Asia simulated by ECHAM6.3 with different schemes of cumulus convective parameterization. *Climate Dynamics*, *54*(9), 4233–4261. https://doi.org/10.1007/s00382-020-05226-1

[12] Abekoon, T., Buthpitiya, B. L. S. K., Sajindra, H., Samarakoon, E. R. J., Jayakody, J. A. D. C. A., Kantamaneni, K., & Rathnayake, U. (2024). A comprehensive review to evaluate the synergy of intelligent food packaging with modern food technology and artificial intelligence field. *Discover Sustainability*, *5*(1), 160. https://doi.org/10.1007/s43621-024-00371-7

[13] Liu, Y., Cheng, A., & Hu, H. (2021). Precipitation simulation from the cumulus convection parameterization schemes based on the WRF model in the Weihe River Basin, China. *Journal of Physics: Conference Series*, *2006*(1), 012004. https://doi.org/10.1088/1742-6596/2006/1/012004

[14] Musa, A. I., Tsubo, M., Ma, S., Kurosaki, Y., Ibaraki, Y., & Ali-Babiker, I.-E. A. (2022). Evaluation of WRF cumulus parameterization schemes for the hot climate of Sudan emphasizing crop growing seasons. *Atmosphere*, *13*(4), 572. https://doi.org/10.3390/atmos13040572

[15] Torsri, K., Faikrua, A., Peangta, P., Sawangwattanaphaibun, R., Akaranee, J., & Sarinnapakorn, K. (2023). Simulating heavy rainfall associated with tropical cyclones and atmospheric disturbances in Thailand using the coupled WRF-ROMS model—Sensitivity analysis of microphysics and cumulus parameterization schemes. *Atmosphere*, *14*(10), 1574. https://doi.org/10.3390/atmos14101574

[16] Kaewmesri, P., Humphries, U., Wangwongchai, A., Wongwies, P., Archevarapuprok, B., & Sooktawee, S. (2017). The simulation of heavy rainfall events over Thailand using microphysics schemes in weather research and forecasting (WRF) model. *World Applied Sciences Journal*, *35*(2), 310–315.

[17] Li, H., Huang, Y., Luo, Y., Xiao, H., Xue, M., Liu, X., & Feng, L. (2023). Does "right" simulated extreme rainfall result from the "right" representation of rain microphysics? *Quarterly Journal of the Royal Meteorological Society*, *149*(757), 3220–3249. https://doi.org/10.1002/qj.4553

[18] Merino, A., García Ortega, E., Navarro, A., Fernandez-Gonzalez, S., Tapiador, F. J., & Sánchez, J. L. (2021). Evaluation of gridded rain-gauge-based precipitation datasets: Impact of station density, spatial resolution, altitude gradient and climate. *International Journal of Climatology*, *41*(5), 3027–3043. https://doi.org/10.1002/joc.7003

[19] de Souza, L. S., da Silva, M. S., de Almeida, V. A., Moraes, N. O., de Souza, E. P., Senna, M. C. A., ..., & Viana, L. Q. (2024). Evaluation of cumulus and microphysical parameterization schemes of the WRF model for precipitation prediction in the Paraíba do Sul River Basin, southeastern Brazil. *Pure and Applied Geophysics*, *181*(2), 679–700. https://doi.org/10.1007/s00024-023-03419-3

[20] Hoogelander, V., Hut, R., Coz, C. L., Dong, J., & van de Giesen, N. (2025). Enhancing rainfall estimates in East Africa by integrating TAHMO ground data and satellite rainfall products. *Journal of Hydrometeorology*, *26*(8), 1063–1087. https://doi.org/10.1175/JHM-D-24-0156.1

[21] Marty, C., Michel, A., Jonas, T., Steijn, C., Muelchi, R., & Kotlarski, S. (2025). SPASS–New gridded climatological snow datasets for Switzerland: Potential and limitations. *The Cryosphere*, *19*(10), 4391–4407. https://doi.org/10.5194/tc-19-4391-2025

[22] Kim, J. H., Jiménez, P. A., Sengupta, M., Dudhia, J., Yang, J., & Alessandrini, S. (2022). The impact of stochastic perturbations in physics variables for predicting surface solar irradiance. *Atmosphere*, *13*(11), 1932. https://doi.org/10.3390/atmos13111932

[23] Park, H. (2024). *Improvement of the scale-adaptive convective parameterization schemes in the simulation of heavy rainfall events over South Korea*. Doctoral Dissertation, Ulsan National Institute of Science and Technology.

[24] Kramer, M., Heinzeller, D., Hartmann, H., van den Berg, W., & Steeneveld, G.-J. (2020). Assessment of MPAS variable resolution simulations in the grey-zone of convection against WRF model results and observations: An MPAS feasibility study of three extreme weather events in Europe. *Climate Dynamics*, *55*(1), 253–276. https://doi.org/10.1007/s00382-018-4562-z

[25] Hokson, J. A., Kanae, S., & Seto, R. (2022). The multi-scale Kain-Fritsch cumulus scheme: Simulating typhoon-induced heavy precipitation over the Philippines. *Journal of Japan Society of Civil Engineers, Ser. G (Environmental Research)*, *78*(5), I_163–I_169. https://doi.org/10.2208/jscejer.78.5_I_163

[26] Qiao, X., Zeng, M., Wang, S., & Zeng, Y. (2023). Impacts of the stochastically perturbed parameterization on the precipitation ensemble forecasts of the Betts–Miller–Janjić (BMJ) scheme in Eastern China. *Atmospheric Research*, *295*, 107036. https://doi.org/10.1016/j.atmosres.2023.107036

[27] Bauer, H.-S., Muppa, S. K., Wulfmeyer, V., Behrendt, A., Warrach-Sagi, K., & Späth, F. (2020). Multi-nested WRF simulations for studying planetary boundary layer processes on the turbulence-permitting scale in a realistic mesoscale environment. *Tellus A: Dynamic Meteorology and Oceanography*, *72*(1), 1761740. https://doi.org/10.1080/16000870.2020.1761740

[28] Jang, J., Skamarock, W. C., Park, S.-H., Zarzycki, C. M., Sakaguchi, K., & Leung, L. R. (2022). Effect of the Grell-Freitas deep convection scheme in quasi-uniform and variable-resolution aquaplanet CAM simulations. *Journal of Advances in Modeling Earth Systems*, *14*(6), e2020MS002459. https://doi.org/10.1029/2020MS002459

[29] Hoque, M. M., Afsar, M. S. U., Faruque, M. R. I., Ahmed, S. J., Jamil, A. K., Mallik, M. A. K., & Hassan, S. Q. (2024). Sensitivity analysis of cumulus parameterization scheme and data sources to simulate thunderstorms over Bangladesh using WRF model. *Advances in Space Research*, *74*(11), 5383–5394. https://doi.org/10.1016/j.asr.2024.08.013

[30] Wang, W. (2022). Forecasting convection with a "scale-aware" Tiedtke cumulus parameterization scheme at kilometer scales. *Weather and Forecasting*, *37*(8), 1491–1507. https://doi.org/10.1175/WAF-D-21-0179.1

[31] Wang, Y., Yang, Z., Ma, J., & Jin, Q. (2024). A wind speed forecasting framework for multiple turbines based on adaptive gate mechanism enhanced multi-graph attention networks. *Applied Energy*, *372*, 123777. https://doi.org/10.1016/j.apenergy.2024.123777

[32] Maddah, M. A., & Mostamandi, S. (2024). WRF prediction of an atmospheric river-related precipitation event: Sensitivity to cumulus parameterization schemes. *Meteorological Applications*, *31*(1), e2160. https://doi.org/10.1002/met.2160

[33] Zhong, X., Yu, X., & Li, H. (2024). Machine learning parameterization of the multi-scale Kain–Fritsch (MSKF) convection scheme and stable simulation coupled in the Weather Research and Forecasting (WRF) model using WRF–ML v1.0. *Geoscientific Model Development*, *17*(9), 3667–3685. https://doi.org/10.5194/gmd-17-3667-2024

[34] Liu, H., Shang, L., Li, M., Zheng, X., & Shi, P. (2024). WRF numerical simulation of summer precipitation and its application over the mountainous southern Tibetan Plateau based on different cumulus parameterization schemes. *Atmospheric Research*, *309*, 107608. https://doi.org/10.1016/j.atmosres.2024.107608

[35] Zhao, Y., Peng, X., Li, X., & Chen, S. (2024). Improved diurnal cycle of precipitation on land in a global nonhydrostatic model using a revised NSAS deep convective scheme. *Advances in Atmospheric Sciences*, *41*(6), 1217–1234. https://doi.org/10.1007/s00376-023-3121-7

[36] Li, J., Gan, Y., Zhang, G., Gou, J., Lu, X., & Miao, C. (2024). Quantifying the interactions of Noah-MP land surface processes on the simulated runoff over the Tibetan Plateau. *Journal of Geophysical Research: Atmospheres*, *129*(7), e2023JD040343. https://doi.org/10.1029/2023JD040343

[37] Altman, N. S. (1992). An introduction to kernel and nearest-neighbor nonparametric regression. *The American Statistician*, *46*(3), 175–185. https://doi.org/10.1080/00031305.1992.10475879

[38] Balaji, T., Mullangi, P., Krishna, G. V., Sujitha, M. J., Bhukya, S., Tumuluru, P., & Undamatla, A. K. (2025). Comparative study of one-class support vector machine, Bayesian network, ridge classifier for meteorological data analysis. *Ingénierie des Systèmes d'Information*, *30*(9), 2365–2374. https://doi.org/10.18280/isi.300913

**How to Cite:** Humphries, U. W., Waqas, M., Archevarahuprok, B., Dechpichai, P., Wangwongchai, A., & Chansawang, B. (2026). High-Resolution Evaluation of WRF Cumulus Parameterization Schemes for Rainfall Prediction in Thailand. *Journal of Data Science and Intelligent Systems*. https://doi.org/10.47852/bonviewJDSIS62027208

## Appendix

### List of Abbreviations

| | |
|---|---|
| WRF | Weather Research and Forecasting |
| TMD | Thai Meteorological Department |
| KNN | K-Nearest Neighbors |
| KF | Kain–Fritsch |
| BMJ | Betts–Miller–Janjic |
| GF | Grell–Freitas |
| RRTMG | Rapid Radiative Transfer Model for General Circulation Models |
| MYJ | Mellor–Yamada–Janjic |
| PBL | Planetary Boundary Layer |
| SBU-YLin | Stony Brook University – YLin Microphysics Scheme |
| NSAS | New Simplified Arakawa–Schubert |
| RMSE | Root Mean Square Error |
| MAE | Mean Absolute Error |
| FAR | False Alarm Ratio |
| HS | Hit Score |
| GoT | Gulf of Thailand |